GLOBAL MHD SIMULATIONS OF THE SUBSTORM CURRENT WEDGE AND DIPOLARIZATION

J. Raeder and R. L. McPherron

Institute of Geophysics and Planetary Physics, University of California, Los Angeles

405 Hilgard Avenue, Los Angeles, CA 90095-1567

Abstract. This paper presents results from global MHD simulations showing the evolution of the plasma and field in the near-Earth tail during the substorm phases. The late growth phase is characterized by pronounced thinning of the plasma sheet and stretching of the field in the region between approximately -6 R_E to -30 R_E. A pre-existing X-line moves tailward to beyond -50 R_E. Close to onset, a new X-line forms near -18 R_E in the midnight sector. Earthward flows emanating from this X-line dipolarize the near-Earth field, leading to a reduction of the cross-tail current in the midnight sector, but not elsewhere. The magnetic shear between the dipolarized field near midnight and the stretched field elsewhere is equivalent to currents flowing through the ionosphere in a region 1 sense, and so forming the current wedge. Later in the expansion phase, the dipolarization spreads in local time at a rate of about 0.3 hours MLT per minute. A strong electric field and a rapid increase of the plasma pressure is associated with the dipolarization. Near midnight the dipolarization appears to occur at all distances between 6.6 and 13 R_E at the same time within the resolution (±2 min) of our model. However, the model results indicate that dipolarization starts *before* ground onset in the pre-midnight sector and propagates both earthward and eastward. Thus, dipolarization may be much more complex than simple earthward/tailward and/or azimuthal expansion.

1. Introduction

The formation of a substorm current wedge at expansion phase onset of a substorm has been known for some time now [*McPherron et al.*, 1973], yet there is still substantial controversy as to its nature. It has been argued that the substorm current wedge forms as a result of flows from a near-Earth X-line, because these flows may not be uniform in the Y-direction, causing magnetic shear of the near-Earth field which is equivalent to currents flowing into and out of the ionosphere [*Birn and Hesse*, 1991; *Birn et al.*, 1996]. A different theory was postulated by [*Lui et al.*, 1988, 1992] which states that processes local to the current wedge itself are responsible for its formation. In this scenario, kinetic instabilities occurring in the near-Earth tail at substorm expansion onset cause a "disruption" of the current in this region. Current continuity then demands that part of the current that was previously flowing across the tail must take a different path, most likely through the ionosphere.

Either mechanism is notoriously difficult to prove or disprove using *in situ* observations, because only single or at most a few spacecraft are available. Too few spacecraft always leave space - time ambiguities and the problem is compounded by the fact that there are significant differences between individual substorms.

In this paper we address the problem by using global simulations. When considering observations of a single spacecraft the simulation results show essentially the same effects as those observed. This indicates that the simulation basically produces the correct physical processes that are responsible for the substorm. We can then interpret the simulation results in their entirety and shed some light on how the substorm process works. Although there are many aspects of substorms that need to be considered, we focus here on the near-Earth tail processes, in particular the dipolarization at onset. Other aspects of this substorm event will be presented elsewhere.

2. The Model

For this study we use our global MHD magnetosphere - ionosphere simulation model that has been used extensively for other studies of the solar wind - magnetosphere - ionosphere interactions in the past. Detailed descriptions of the model can be found in [*Raeder et al.*, 1996, 1997, 1998]. Thus we give only a brief description of the model parameters pertaining to this study. The resistive MHD equations are solved on a nonuniform rectangular grid extending from $X_{GSE} = $ -300 to $X_{GSE} = 22$ R_E, and from -40 R_E to 40 R_E in the transverse directions, thus placing all outer boundaries into supermagnetosonic flows. The grid resolution is about 0.35 R_E near the Earth and increases towards the boundaries of the simulation box. Magnetospheric Birkeland currents are closed by using an ionosphere model that computes the ionospheric potential from the Birkeland currents. The ionospheric Hall and Pedersen conductances are computed by using an empirical model for EUV ionization [*Moen and Brekke*, 1993], and by using self-consistently computed diffuse and discrete electron precipitation. This run was started about 5 hours before the event under consideration. The first

two hours a steady negative IMF B_z was used, after that the measured solar wind parameters were used.

3. Results

Here we present simulation results for a substorm that occurred on May 19, 1996 at around 2028 UT. The simulation was driven by solar wind and IMF data obtained by the Wind satellite. The results of this simulation were compared with ground observations and with magnetic field observations in the southern tail lobe obtained by IMP-8. The comparisons showed by and large a good correlation between the simulation results and the data. In particular, the simulation results show a substorm onset at about 2028 UT in the simulated ground magnetometers that corresponds well with the observed ground magnetometer signatures. Details of these comparisons will be presented elsewhere.
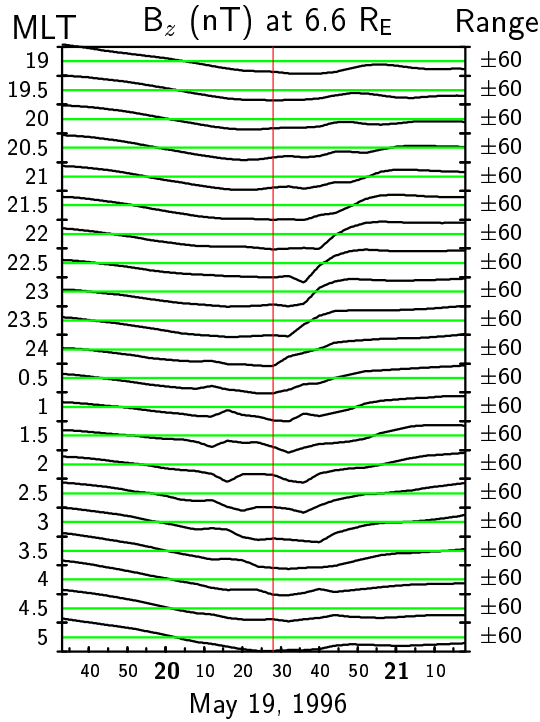

Figure 1: The B_z component of the magnetic field in the magnetic equatorial plane at geosynchronous distance and at different magnetic local times. For each trace the median value has been subtracted.

3.1. Spreading of the Dipolarization

Figure 1 shows the magnetic field B_z component in the tail from the simulation as it would be seen by a number of satellites in the magnetic equator at geosynchronous orbit. These virtual satellites span magnetic local times from 5 MLT to 19 MLT. The expansion phase onset as determined from the simulated ground magnetic signatures is indicated by the vertical line at 2028 UT. Within 2 minutes of the onset, the virtual spacecraft located at 24 MLT observes a
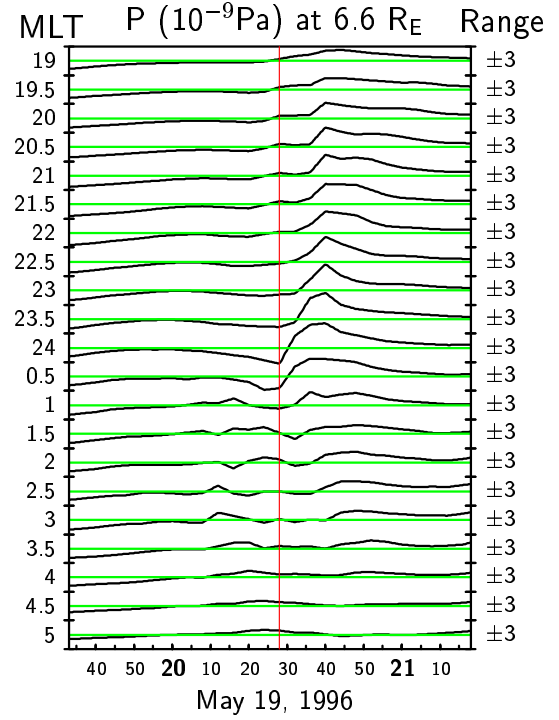

Figure 2: The plasma pressure in the magnetic equatorial plane at geosynchronous distance and at different magnetic local times. For each trace the median value has been subtracted.
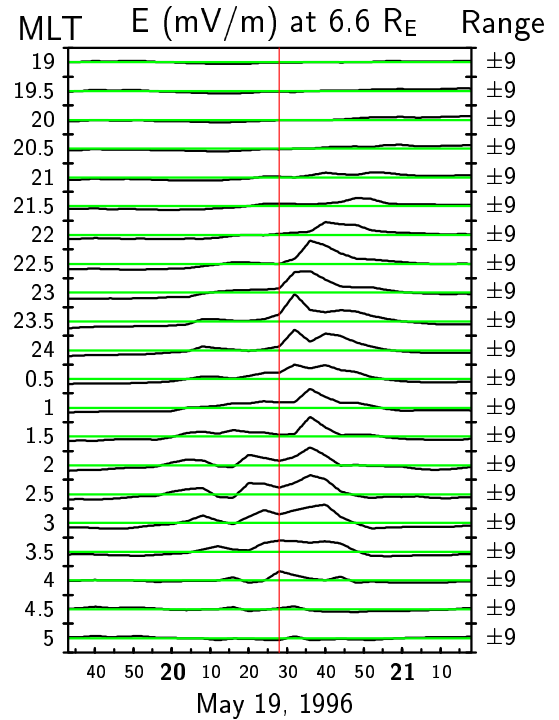

Figure 3: The total electric field in the magnetic equatorial plane at geosynchronous distance and at different magnetic local times. For each trace the median value has been subtracted.

rapid increase in B_z. A similar B_z increase can be seen at later times at almost all other virtual spacecraft. Clearly, the

rapid B_z increase indicates the dipolarization of the magnetic field. The dipolarization begins at local midnight and then spreads azimuthally at a rate of about 0.3 hours MLT per minute. This rate is comparable to, albeit somewhat slower, than the rate that was found by *Nagai* [1982] in a statistical study. The field dipolarization is generally stronger in the pre-midnight sector and peters out after about 4 hours MLT on either side of the midnight meridian. The fastest dipolarization rate occurs at 22.5 MLT and has a value of about 20 nT/min. This value is consistent with observations near geosynchnonous altitude [**?**].

Figure 2 shows the plasma pressure for the same configuration of virtual spacecraft as in Figure 1. A rapid pressure increase occurs almost simultaneously with the increase of B_z. The pressure increase is strongest near midnight and weakest post-midnight. It is also noticeable that the pressure increase in the pre-midnight sector between 19 and 22 MLT occurs several minutes before the dipolarization.

Figure 3 shows the total electric field for the same configuration of virtual spacecraft as in Figure 1. A substantial increase of the electric field occurs at the same time as the B_z values increase. The peak value of the electric field increase (20 mV/m) compares well with observations. *Shepherd et al.* [1980] found peak values of 15 mV/m for a similar sized event, while for a much larger event 60 mV/m were reported [*Aggson et al.*, 1983]. There is already a noticeable increase of the electric field values before the dipolarization occurs, indicating that some tail reconfiguration occurs prior to the expansion phase onset. Unlike the pressure increases, the electric field pulses are stronger in the pre-midnight sector.
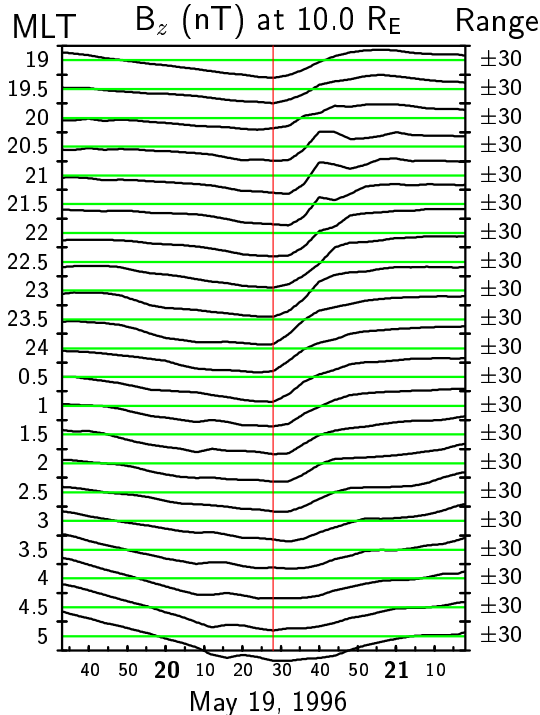

Figure 5: The B_z component of the magnetic field in the magnetic equatorial plane at 13 R_E distance and at different magnetic local times. For each trace the median value has been subtracted.
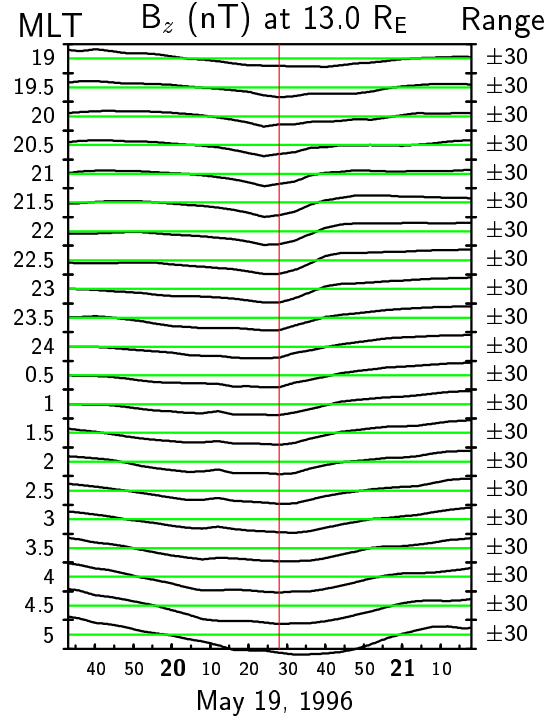
Figures 4 and 5 show the magnetic field B_z component in the tail similar to Figure 1, but at 10 and 13 R_E from Earth, respectively. The field signature is basically the same as at 6.6 R_E but less pronounced. Comparing the 24 MLT time traces of Figures 1, 4, and 5 one finds that the dipolarization onset occurs at the same time regardless of the distance from Earth. In other words, there appears to be no propagation of a dipolarization front near midnight, neither earthward nor tailward. One should note, however, that the time resolution of the simulation is limited to about ± 2 minutes, thus there may indeed be a propagation that is not resolved in this simulation. In the pre-midnight sector, however, there are clear signs of a beginning field dipolarization *before* the ground onset and before the dipolarization onset at midnight. Between 2000 and 2200 MLT a dipolarization front propagates earthward and possibly dawn ward.

Figure 6 shows three-dimensional views of the tail configuration at three different times. All three panels show the same perspective; the look angle is from 3.5 hours MLT and 15° elevation. The panels show color coded the x-component of the velocity (V_x) in a plane that is offset by 3 R_E from the noon-midnight meridian toward dusk. Blue and purple color tones indicate antisunward flow, red and yellow tones indicate sunward flows, and green tones indicate very slow velocity values. The red surface is the isocontour of $V_x = 200$ km/s, i.e., the accelerated sunward flows. The yellowish surface is the isocontour of 800 pico Pascal plasma pressure. The red field lines originate in the ionosphere at the magnetic noon-midnight meridian. The blue field lines originate in the ionosphere at 65° magnetic latitude. The large

Figure 4: The B_z component of the magnetic field in the magnetic equatorial plane at 10 R_E distance and at different magnetic local times. For each trace the median value has been subtracted.

blue sphere represents the inner boundary of the simulation at 3.7 R_E.

The top panel (6a) shows the tail configuration during the late growth phase at 2020 UT, 8 minutes before expansion phase onset. There is a X-line present in the tail beyond about -40 R_E (not visible in this figure). The tail field is highly stretched and the flux tubes exhibit strong kinks in the magnetic equator. This region of a strong cross tail current sheet reaches from well inside geosynchronous distance to beyond -30 R_E. Field lines near geosynchronous distances and tailward of the terminator (the blue field lines in the figure) are all highly stretched and deviate considerably from a dipolar field. The flow is earthward directed and the flow velocity values are relatively small. The strongest flows look like plasma sheet boundary layer (PSBL) flows, i.e., they are predominantly parallel to the field and divert around the inner magnetosphere to high latitudes. This flow is essentially the fluid counterpart to the PSBL ion beams that are frequently observed [*Eastman and Hones*, 1979; *Eastman et al.*, 1985]. The 800 pPa contour surface of the plasma pressure outlines the shape of the plasma sheet in the near-Earth region. At this time, the plasma sheet is considerably compressed and shows a sharp kink, i.e., large pressure gradient, at the equator.

The second panel (6b) of Figure 6 shows the tail configuration approximately 8 minutes after expansion phase onset. A new X-line has formed at about -18 R_E near the noon-midnight meridian. From this X-line strong flows emerge both earthward and tailward. The earthward flow, which barely exceeded 200 km/s during the growth phase now reaches values as high as 700 km/s. Also, the flow is not PSBL-like any more, but has a large component that is perpendicular to the field. As a consequence, magnetic flux is rapidly transported earthward and the field near the meridian dipolarizes. However, at this time the X-line is still of very limited extent in the Y-direction. Thus the field lines that are not close to the meridian are still stretched (see the blue field lines in the nightside). This causes substantial magnetic shear between the dipolarized and the stretched field which is equivalent to a (mostly) field aligned current. This current is in the region 1 current sense, i.e., it flows into the ionosphere at the dawn side and out of the ionosphere in the dusk side.

The third panel of Figure 6 (6c) shows the tail configuration about 90 minutes after onset. At this time the field is dipolarized at all local times, thus the current wedge ceases to exist. Together with the dipolarized field, the plasma sheet has become thicker and symmetric. The X-line has somewhat retreated to -20 R_E. The fact that the X-line is still close to the Earth may be attributed to the IMF which has in this case not yet returned to a northward orientation.

4. Summary and Conclusions

We have used a global MHD simulation of an isolated substorm event to study the spatial and temporal evolution of the substorm current wedge and the magnetic field dipolarization.

We find that at geosynchronous distance the field dipolarization starts near local midnight, coincident with the ionospheric onset signatures of the model, i.e., a sudden drop of AL and rapid increase of discrete electron precipitation (not shown here). The dipolarization then spreads both eastward and westward at a rate of about 0.3 hours MLT/min. This value is consistent with the findings of a statistical study [*Nagai*, 1982] in which a value of about 0.5 hours MLT/min was determined. However, in *Nagai's* study the spreading rate was obtained using superposed epoch analysis, thus leaving room for time - space ambiguity. Our study clearly shows that the spreading, i.e., the increasing time difference between expansion phase onset and the beginning of the field dipolarization as a function of azimuthal distance from local midnight, is indeed caused by the azimuthal expansion of a dipolarization front.

The model results are less clear, however, with respect to a radial propagation of a dipolarization front. Near local midnight there appears to be no propagation either way. However, this lack of propagation may just be buried in the limited time resolution of the model. The situation is more complicated if one looks at different local times. Around 2100 MLT and 13 R_E distance, dipolarization starts *before* the ground onset and then propagates earthward. However, at this local time, the increase of B_z is strongest around 10 R_E, and only very weak at 6.6 R_E. It thus appears that a dipolarization front starts in the pre-midnight sector before ground onset, and then first propagates earthward and duskward. At onset, more rapid dipolarization then occurs at all distances considered here at local midnight and spreads azimuthally in both directions.

In summary, our findings are generally consistent with the near Earth neutral line model of substorms. Current wedge formation and field dipolarization are caused by the formation of a new neutral line before onset and the resulting fast earthward flows. The limited resolution of our simulations do not allow us yet to determine the propagation of the dipolarization front with sufficient precision. However, our results indicate that the dipolarization may be more complex than simple earthward/tailward and/or azimuthal propagation and that the propagation direction may actually change during the expansion phase. This may explain why it has been so difficult in the past to determine the propagation direction without ambiguity by using *in situ* observations.

References

Aggson, T. L., J. P. Heppner, and N. C. Maynard, Observations of large magnetospheric electric fields during the onset phase of a substorm, *J. Geophys. Res.*, *88*, 3981, 1983.

Birn, J., and M. Hesse, The substorm current wedge and field

aligned currents in MHD simulations of magnetotail reconnection, *J. Geophys. Res.*, *96*, 1611, 1991.

Birn, J., M. Hesse, and K. Schindler, MHD simulations of magnetotail dynamics, *J. Geophys. Res.*, *101*, 12,939, 1996.

Eastman, T. E., and E. W. Hones, Characteristics of the magnetospheric boundary layer and magnetopause layer as observed by IMP 6, *J. Geophys. Res.*, *84*, 2019, 1979.

Eastman, T. E., L. A. Frank, and C. Y. Huang, The boundary layers as the primary transport regions of the Earth's magnetotail, *J. Geophys. Res.*, *90*, 9541, 1985.

Lui, A. T. Y., R. E. Lopez, S. M. Krimigis, R. W. McEntire, L. J. Zanetti, and T. A. Potemra, A case study of magnetotail current sheet disruption and diversion, *Geophys. Res. Lett.*, *15*, 721, 1988.

Lui, A. T. Y., et al., Current disruptions in the near-Earth neutral sheet region, *J. Geophys. Res.*, *97*, 1461, 1992.

McPherron, R. L., C. T. Russell, and M. P. Aubry, Satellite studies of magnetospheric substorms on August 15, 1968, 9. Phenomenological model for substorms, *J. Geophys. Res.*, *78*, 3131, 1973.

Moen, J., and A. Brekke, The solar flux influence on quiet time conductances in the auroral ionosphere, *Geophys. Res. Lett.*, *20*, 971, 1993.

Nagai, T., Observed magnetic substorm signatures at synchronous altitude, *J. Geophys. Res.*, *87*, 4405, 1982.

Raeder, J., J. Berchem, and M. Ashour-Abdalla, The importance of small scale processes in global MHD simulations: Some numerical experiments, in *The Physics of Space Plasmas*, edited by T. Chang and J. R. Jasperse, vol. 14, p. 403, MIT Cent. for Theoret. Geo/Cosmo Plasma Phys., Cambridge, Mass., 1996.

Raeder, J., J. Berchem, and M. Ashour-Abdalla, GGCM modeling of ionospheric convection: The GEM Grand Challenge, *J. Geophys. Res.*, *103*, in press, 1998.

Raeder, J., et al., Boundary layer formation in the magnetotail: Geotail observations and comparisons with a global MHD model, *Geophys. Res. Lett.*, *24*, 951, 1997.

Shepherd, G. G., et al., Plasma and field signatures of poleward propagating auroral precipitation observed at the foot of the GOES 2 field line, *J. Geophys. Res.*, *85*, 4587, 1980.
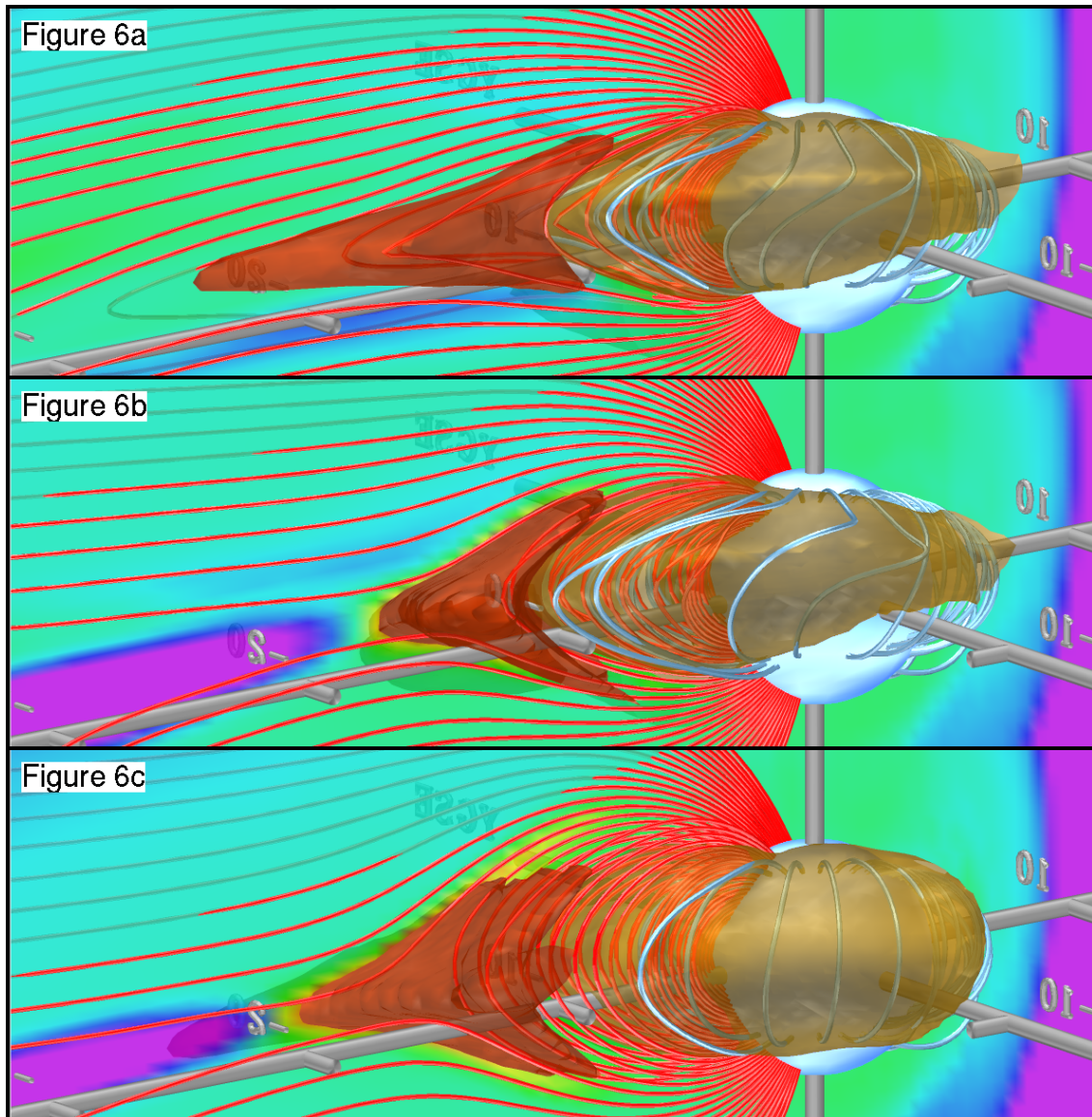
Figure 6a-c.   Three-dimensional rendering of the magnetosphere at three different times. 6a) late growth phase, 6b) immediately after expansion phase onset, 6c) during the recovery phase. In all three figures the look angle is from 3.5 hours MLT and 15° elevation. The figures show color coded the x-component of the velocity (V_x) in a plane that is offset by 3 R_E from the noon-midnight meridian toward dusk. Blue and purple color tones indicate antisunward flow, red and yellow tones indicate sunward flows, and green tones indicate very slow velocity values. The red surface is the isocontour of $V_x = 200$ km/s. The yellowish surface is the isocontour of 800 pico Pascal plasma pressure. The red field lines originate in the ionosphere at the magnetic noon-midnight meridian. The blue field lines originate in the ionosphere at 65° magnetic latitude. The large blue sphere reperesents the inner boundary of the simulation at 3.7 R_E.

Figure 6: